High-throughput small molecule screen identifies inhibitors of microsporidia invasion and proliferation in *C. elegans*.

Brandon M. Murareanu[1], Jessica Knox[1,2], Peter J. Roy[1,2], Aaron W. Reinke[1#].

[1]Department of Molecular Genetics, University of Toronto, Toronto, ON, Canada

[2]The Donnelly Centre for Cellular and Biomolecular Research, University of Toronto, Toronto,

#Corresponding author

aaron.reinke@utoronto.ca

Abstract

Microsporidia are a diverse group of fungal-related obligate intracellular parasites that infect most animal phyla. Despite the emerging threat that microsporidia have become to humans and agricultural animals, few reliable treatment options exist. To identify novel chemical inhibitors of microsporidia infection, we developed a high-throughput screening method using *Caenorhabditis elegans* and the microsporidia species *Nematocida parisii*. We screened the Spectrum Collection of 2,560 FDA-approved compounds and natural products to identify compounds that prevent *C. elegans* progeny inhibition caused by *N. parisii* infection. We developed a semi-automated method for quantifying *C. elegans* progeny number in liquid culture, confirming 11 candidate microsporidia inhibitors. We show that five compounds prevent microsporidia infection by inhibiting spore firing, and demonstrate that one compound, dexrazoxane, slows infection progression. Together, our results demonstrate the effectiveness of *C. elegans* as a model host for drug discovery against intracellular pathogens and provide a scalable high-throughput system for the identification and characterization of additional microsporidia inhibitors.

Introduction

Microsporidia are a diverse group of parasites, comprising over 1400 species that can infect most major animal phyla (1–3). Many microsporidia species infect agriculturally important animals. This includes invertebrate-infecting species such as *Nosema ceranae* and *Nosema apis* which infect honey bees, *Enterocytozoon hepatopenaei* which infects shrimp, *Hepatospora eriocheir* which infects crabs, and *Nosema bombycis* which infects silkworms (4–7). Additionally, there are several species that infect farmed fish, including *Loma salmonae* which infects salmon and trout, as well as *Enterospora nucleophila* which infects gilthead sea bream (8, 9). Microsporidia infection in these animals can result in reduced body size, fewer offspring, and increased mortality (4–9). The economic impact of microsporidia infections is high. The infection of silkworms has triggered historical collapses of the sericulture industry, and microsporidia infections are estimated to cost over $200 million USD annually to Thailand's shrimp industry (7, 10). Livestock such as pigs, cattle, and sheep, as well as pets such as dogs, cats and rabbits are infected by *Encephalitozoon* species and *Enterocytozoon bieneusi*. Humans are also infected by these species, with infections in the immunocompromised being more prevalent (11). Microsporidia commonly infect animals, with over half of honeybee hives and approximately 40% of pigs reported to be infected (11, 12). Microsporidia are also emerging pathogens, with the threat posed by many of these species only being recognized in the last several decades (13).

Despite the threat that these parasites pose to human and animal health, few therapeutic options exist. Fumagillin is a compound from the fungus *Aspergillus fumigatus* which inhibits methionine aminopeptidase type 2 (MetAP2), and has been used since the 1950s to treat microsporidia infections in honeybees (14). However, recent reports suggest that fumagillin may be ineffective against *N. ceranae* in honeybees and *E. hepatopenaei* in shrimp (15, 16). In addition, fumagillin causes toxicity in humans and its use in beekeeping is banned in some countries (17). The other most used therapeutic agent against microsporidia is albendazole, which disrupts β-tubulin function. Several microsporidia species, including *E. bieneusi,* have β-tubulin variants associated with albendazole resistance, and as a result, these species are not susceptible to the drug (18). Several other approaches for the drug treatment of microsporidia infections have been described, including inhibition of chitin synthase, as

well as inhibition of spore firing by blocking calcium channels (18, 19). Microsporidia only grow inside of host cells, making screening for inhibitors challenging. Several screens to identify microsporidia inhibitors have been performed, but these have been limited to less than 100 compounds at a time due to a lack of applicable high-throughput screening assays (20, 21).

The model organism *Caenorhabditis elegans* is a powerful system to study infectious diseases and is widely amenable to high-throughput drug screens. *C. elegans* is commonly infected in nature by the microsporidian *Nematocida parisii,* which has been used as model to study microsporidia spore exit, host immunity, and proteins used by microsporidia to interact with its host (22–26). The infection of *C. elegans* begins when *N. parisii* spores are ingested. Spores then germinate in the intestinal lumen, where their unique invasion apparatus known as a polar tube is fired, enabling sporoplasm deposition into intestinal epithelial cells (27, 28). Intracellularly, sporoplasms grow into meronts and differentiate into spores, which then exit the worm, with over 100,000 spores being produced by each infected animal (29). Infection of *C. elegans* by *N. parisii* results in impaired growth, reduced progeny production, and lethality (23, 27). The ease of culturing and growing large numbers of animals, along with easily discernible phenotypes, has made *C. elegans* a powerful platform to identify novel anthelmintic, antibiotic, and antifungal agents (30–37).

To discover additional microsporidia inhibitors, we used the *C. elegans / N. parisii* model system to develop a high-throughput, liquid-based drug screening assay in which compounds were scored for their ability to prevent infection-induced progeny inhibition. Using this assay, we screened the Spectrum Collection of 2,560 FDA-approved compounds and natural products, and identified 11 chemical inhibitors of microsporidia infection, which we confirmed using a semi-automated method for quantifying *C. elegans* progeny number in liquid culture. We report that five of these compounds, including the known serine protease inhibitor ZPCK and four compounds that share a quinone structure, prevent microsporidia invasion in *C. elegans* by inhibiting spore firing. Additionally, the iron chelator and topoisomerase II inhibitor dexrazoxane prevents infection progression. Together, this work describes

methods to screen thousands of putative microsporidia inhibitors and identifies novel microsporidia inhibitors that either block microsporidia invasion or proliferation.

Results

High-throughput screen of 2,560 Spectrum Collection compounds reveals 11 microsporidia inhibitors

To identify inhibitors of microsporidia infection, we developed a novel screening assay for chemical inhibitors based on the observation that *C. elegans* progeny production is greatly inhibited when infected with *N. parisii* (23, 38). In our screening assay, L1 animals in 96-well plates were grown in liquid and infected with *N. parisii* spores for six days at 21ºC (Fig. 1A, see methods). In the absence of *N. parisii* spores, *C. elegans* larvae develop into adults and produce progeny. In the presence of spores, the animals are smaller and produce fewer progeny, providing a convenient visual indication of infection. This inhibition of progeny production is prevented by the known microsporidia inhibitor fumagillin (Fig. 1B). Using this assay, we tested 2,560 FDA-approved compounds and natural products from the Spectrum Collection for their ability to prevent infection-induced progeny inhibition. After incubation with compounds for six days, each well was visually assessed for *C. elegans* progeny production. We identified 25 initial compounds that when added to wells, resulted in the production of more progeny than the vehicle, DMSO, controls. Upon retesting, 11 compounds were confirmed to reproducibly restore *C. elegans* progeny production in the presence of spores (Table S1).

To quantify the inhibitory effect of each compound, we developed a semi-automated approach to quantify progeny number in liquid culture, (Fig. 1A, see methods). Animals were grown in wells as described above, stained with the dye rose bengal, and imaged using a flatbed scanner. Images were processed with consistent parameters to highlight stained animals and analyzed with WorMachine to detect and count the number of animals in each well (Fig. S1A-C) (39). Counts of animals detected using WorMachine correlated well with those counted manually (Fig. S1D). Additionally, there was good

correlation (average R^2 of 0.71) between technical replicates (Fig. S1E). This approach is similar to a recently published method, but with the advantage of using a relatively cheap flatbed scanner for imaging (40–42). We observed that each of the 11 compounds was able to significantly increase the number of progeny produced by animals under infection conditions (Fig. 1C). This effect is even more pronounced when considering that for six of the compounds, there was a significant reduction in progeny production in uninfected animals, indicating moderate host toxicity (Fig. 1D).

Our initial screen identified compounds that could rescue the ability of *C. elegans* to produce progeny in the presence of *N. parisii* spores. To determine whether the compounds have a direct effect on microsporidia infection, we performed continuous infection assays. L1 animals were infected continuously with *N. parisii* spores in the presence of compounds for 4 days at 21ºC in 24-well plates in liquid (Fig. 2A). After incubation, animals were fixed and stained with direct yellow 96 (DY96), a fluorescent dye that binds chitin, a crucial component of both the microsporidia spore wall and *C. elegans* embryos (Fig. 2B) (43, 44). First, we observed that every compound significantly increased the proportion of adult animals containing embryos in the presence of *N. parisii* spores (Fig. 2C). These results are consistent with our data from the initial screen showing that all compounds increased progeny production in the presence of spores (Fig. 1C). Second, we determined that the control inhibitor fumagillin and 9 of the 11 compounds inhibited microsporidia infection, as the proportion of animals with newly formed spores was significantly lower upon treatment with these compounds (Fig. 2D).

N. parisii **proliferation is inhibited by dexrazoxane**

Microsporidia infection can be inhibited either by blocking invasion, or by preventing proliferation after infection is established. To distinguish between these possibilities, we performed pulse-chase infection assays where L1 animals were infected with *N. parisii* spores for 3 hours, washed to remove excess spores, and incubated with compounds for 4 days (Fig. 3A). As expected, given its described mode of action as a MetAP2 inhibitor (17), fumagillin restricted *N. parisii* proliferation (Fig 3B). Surprisingly, of

our 11 compounds, only one, dexrazoxane, inhibited *N. parisii* proliferation (Fig. 3E). Both fumagillin and dexrazoxane restored the ability of animals to make embryos when infected, whereas none of the other compounds were able to do so (Fig. 3D). The effect of dexrazoxane, at a concentration of 60 μM, is especially striking with a ~1200-fold reduction in the proportion of animals with newly-formed spores, compared to just ~2-fold for fumagillin, at a concentration of 350 μM (Fig. 3E). Together, these results suggest that of the compounds identified from our screen, only dexrazoxane inhibits *N. parisii* after invasion of *C. elegans* has occurred.

To determine whether dexrazoxane inhibits microsporidia by slowing proliferation or enhancing parasite clearance, we used FISH staining of pulse-chase infected animals with probes specific for *N. parisii* 18S RNA to visualize the sporoplasms and meronts of the earlier stages of infection prior to new spore formation (27). Although fumagillin and dexrazoxane both resulted in many fewer animals with newly formed spores (Fig. 3E), there was no significant difference in the proportion of animals that had at least some FISH signal (Fig. 3F). When *C. elegans* is pulse-chase infected with *N. parisii* for 48 h, many large, multinucleated meronts are observed. Worms treated with fumagillin contain both large meronts with many nuclei as well as some parasite cells that fail to progress beyond having 2 nuclei. In contrast, dexrazoxane treatment leads to almost all parasite cells containing 1 or 2 nuclei, and many parasite cells displaying irregular morphology (Fig. 3C). Using images of FISH-stained *N. parisii*, we quantified the area of the infected animal that is covered by sporoplasms and meronts. We observed that fumagillin and dexrazoxane treatment resulted in a significantly reduced pathogen load, with dexrazoxane having the strongest effect (Fig. 3G). Together, these results indicate that dexrazoxane can greatly inhibit *N. parisii* proliferation but does not cause the infection to be cleared.

Dexrazoxane is an iron chelator, and iron levels have been shown to impact the growth of other microsporidia species (45, 46). To determine if iron levels are important for *N. parisii* growth in *C. elegans*, we supplemented our liquid cultures with ferric ammonium citrate (FAC) as a water-soluble iron source (47), and continuously infected L1 animals with a low dose of spores for 4 days. While the

proportion of animals with newly formed spores was slightly higher in the supplemented condition, this effect was not statistically significant (Fig. S2A). In contrast, addition of FAC resulted in a small, but significant increase in the proportion of animals containing embryos (Fig. S2B). To determine whether dexrazoxane is likely acting as an iron chelator in our system, we tested another iron chelator, 2,2'-bipyridyl (BP), for anti-microsporidial activity in our continuous infection assay, but did not observe an effect (Fig. 3H and S2C). In addition, FAC supplementation was unable to counteract the anti-microsporidial effect of dexrazoxane (Fig. 3H and S2C). We also tested the *smf-3(ok1035)* mutant strain RB1074 for sensitivity to dexrazoxane. RB1074 has ~50% less iron levels compared to the wild-type N2 strain and displays a striking growth defect upon treatment with the iron chelator BP (47). However, RB1074 did not display any such growth impairment upon treatment with dexrazoxane (Fig. S3). Taken together, these results demonstrate that the inhibitory effect of dexrazoxane on *N. parisii* infection is likely independent of its established function as an iron chelator.

Protease inhibitors and quinone derivatives prevent invasion by inhibiting spore firing

Compounds that displayed strong activity against microsporidia infection in the continuous infection assays, but not the pulse-chase infections, may be preventing invasion by inhibiting spore firing. In *C. elegans*, *N. parisii* spores are ingested, and spore firing is triggered in the intestinal lumen (27, 48). To test if any compounds interfere with this process, we performed spore firing assays on the 7 compounds with the strongest effect in the continuous infection assays (Fig. 2D). L1 stage *C. elegans* were infected with *N. parisii* for 3 hours, and then stained with FISH and DY96 (Fig. 4A). This dual staining enables us to determine whether a given spore in the intestine has fired, based on whether it has released its sporoplasm (Fig. 4C). We found that treatment with five compounds (ZPCK, menadione, plumbagin, thymoquinone and dalbergione) resulted in a significantly reduced proportion of fired spores in the intestine (Fig. 4D). Treatment with these compounds, as well as chloranil, also lead to a notable reduction in the number of sporoplasms per animal (Fig. 4E). The two compounds that inhibit microsporidia proliferation, fumagillin and dexrazoxane, had no significant effect on spore firing,

although fumagillin treatment did result in a significant decrease in sporoplasm numbers (Fig. 4D and E).

ZPCK is an irreversible inhibitor of serine proteases, and a microsporidia serine protease has previously been suggested to be involved in spore firing (49, 50). To determine if other serine protease inhibitors can prevent *N. parisii* invasion, we tested three additional small molecules (TPCK, TLCK and PMSF) and three peptides (Antipain, Chymostatin and Leupeptin) known to inhibit serine proteases in a modified version of our spore firing assay. For these experiments, we incubated spores with serine protease inhibitors for 24 hours to accentuate their effects, and then used the spores to infect L1 stage *C. elegans* for 3 hours in the presence of inhibitors (Fig. 4B). Analysis of the proportion of spores fired and the number of sporoplasms per animal revealed that both ZPCK and the structurally related inhibitor TPCK displayed strong inhibition of *N. parisii* spore firing and invasion (Fig. 4F and G).

Inhibitors of spore firing could function either by inhibiting an *N. parisii* spore protein or a *C. elegans* protein necessary for firing and invasion. To distinguish between these possibilities, we incubated spores for 24 hours with each of the compounds that inhibited spore firing, washed away excess inhibitor, and then used the treated spores to infect L1 stage *C. elegans* for 3 hours in the absence of inhibitors (Fig. 4B). Treatment with all 6 inhibitors (ZPCK, TPCK, menadione, plumbagin, thymoquinone and dalbergione) significantly inhibited spore firing and sporoplasm invasion (Fig. 4H and I). These results demonstrate that all of these inhibitors act directly on *N. parisii* spores to prevent firing and invasion, and in the case of ZPCK and TPCK, this likely occurs through the inhibition of a serine protease.

Discussion

To identify inhibitors of microsporidia, we screened 2,560 compounds for their ability to counteract infection-induced *C. elegans* progeny inhibition. We identified 11 compounds with reproducible inhibitory activity (Table S1). We found that dexrazoxane inhibits *N. parisii* proliferation, whereas the

protease inhibitors ZPCK and TLCK, along with 4 quinone derivatives, prevent spore firing and invasion (Fig. 5). Three of the identified inhibitors, curcumin, plumbagin, and thymoquinone, have been previously shown to inhibit microsporidia infection, although in the case of plumbagin and thymoquinone, the compounds were effective after microsporidia had infected cells (20, 21). This contrasts with our results, where these compounds only prevent microsporidia invasion. To our knowledge none of the other compounds we identified have been previously reported to prevent microsporidia infection, demonstrating the value in this unbiased approach to identify novel microsporidia inhibitors.

Dexrazoxane is an FDA-approved drug for the prevention of cardiomyopathies caused by chemotherapeutic drugs in cancer patients (51). Dexrazoxane can be hydrolyzed into a structure that is similar to the metal ion chelator ethylenediaminetetraacetic acid and is thought to work by reducing the amount of iron complexed with anthracycline chemotherapeutics, thus reducing the number of superoxide radicals formed by such interactions (52, 53). Iron is an important metabolite for microsporidia proliferation. Honey bees infected with *N. ceranae* have reduced levels of iron and the growth of *E. cuniculi* in macrophages was promoted with the addition of iron and inhibited upon addition of an iron chelator (45, 46). We found that dexrazoxane could prevent microsporidia proliferation, at a concentration that has little effect on host fitness. Given the established role of dexrazoxane as an iron chelator, it seemed likely that its mechanism as an anti-microsporidial might involve sequestering iron away from sporoplasms and meronts, thus depriving them of a crucial resource required for growth and infection progression. However, our results do not support this. Neither treatment with the iron chelator BP, nor iron supplementation using FAC, had any significant effect on *N. parisii* infection. Additionally, dexrazoxane still exhibited strong anti-microsporidial effects when *C. elegans* were exposed to *N. parisii* in a high iron environment. These results suggest that the anti-microsporidial properties of dexrazoxane are unlikely to be the result of drug-induced alterations in iron homeostasis. This is contrast to lethality of *C. elegans* caused by the pathogenic bacteria *Pseudomonas aeruginosa*, which can be reversed by treatment with the iron chelator ciclopirox olamine, which was included in our

screen, but was not observed to have an effect against *N. parisii* (54). The iron chelator desferoxamine, which inhibits *E. cuniculi* in macrophages, was also included in our screen, but not observed to have activity against *N. parisii* (46). A second proposed mechanism for dexrazoxane is the inhibition of topoisomerase II (55). However, several topoisomerase II inhibitors that have previously been used with *C. elegans* (etoposide, teniposide, dactinomycin, and amsacrine), were included in our initial screen, but were not observed to have activity against *N. parisii* (56). The mechanism of action of dexrazoxane in blocking *N. parisii* proliferation thus remains elusive.

The proteins that control spore firing in microsporidia are unknown (57, 58). Although the *in vivo* signal for firing is undetermined, several different pH and salt conditions can trigger firing *in vitro* (57). Once microsporidia spores are exposed to a host signal, the osmotic pressure of the spore increases forcing the polar tube to be extruded. One protein hypothesized to control spore firing is the subtilisin serine protease which is conserved throughout microsporidia (58). This protein localizes to the poles of *N. bombycis* spores, and the activated version of the protease localizes to the end of the spore from which the polar tube fires (59). Here we show that two irreversible serine protease inhibitors (ZPCK and TPCK) can block firing and prevent invasion. Additionally, we identified four quinone derivatives (menadione, plumbagin, thymoquinone and dalbergione) that also block firing and invasion. For all six of these spore firing inhibitors, we observed that firing is still blocked even when the compounds are washed away following their use in the pre-treatment of spores. These results demonstrate that the inhibitors likely act directly on the spores to irreversibly block firing, even when the trigger for firing occurs inside of the host animal. As spore firing is the initial step in invasion, blocking spore firing is a promising potential strategy to prevent microsporidia infections in agricultural animals.

The *C. elegans* / *N. parisii* system provides a powerful tool to both uncover and characterize novel microsporidia inhibitors. Our approach is high-throughput, relatively cheap and scalable, allowing the screening of even more diverse collections of small-molecule libraries (60). Our screen is advantageous as it is performed with wild-type animals and pathogens, and by screening based on

host fitness, this approach only identifies compounds with minimal host toxicity (35). C. elegans is also infected by several other microsporidia in addition to *N. parisii*, including a species that is related to the human infecting microsporidia *Enterocytozoon bieneusi*, providing the opportunity to test the specificity of compound inhibition on multiple species of microsporidia (22). As evidenced by our results, *C. elegans* is a very useful host for determining at what stages of microsporidia infection the identified inhibitors are acting (23). *C. elegans* is also likely to be useful for future work generating *N. parisii* strains with evolved resistance to these inhibitors. The isolation of resistant variants is a promising strategy to identify inhibitor targets, which has been done successfully with other eukaryotic parasites (61, 62).

Acknowledgements

We thank Hala Tamim El Jarkass and Alexandra R. Willis for providing helpful comments on the manuscript and Hala Tamim El Jarkass for the illustration in figure 5. This work was supported by the Natural Sciences and Engineering Research Council of Canada Undergraduate Student Research Awards (to B.M.), Canadian Institutes of Health Research grant no. 400784 (to A.R.), 173448 (to P.R) , and 313296 (to P.R.), Centre for Collaborative Drug Research pilot project fund (to A. R.), Connaught New Researcher Award (to A.R.), an Alfred P. Sloan Research Fellowship FG2019-12040 (to A.R.), and Canada Research Chair award (to P.R.). Some strains were provided by the CGC, which is funded by NIH Office of Research Infrastructure Programs (P40 OD010440) and we thank WormBase.

Author contributions: B.M., J. K., A.R., and P.R. designed the inhibitor screen. B.M. performed all of the experiments. B.M and A.R. analyzed the data and co-wrote the paper with edits from P.R. and J.K.

Competing Interests: The authors declare that they have no competing interests.

Methods

Chemical sources

The Spectrum Collection of FDA-approved compounds and natural products was obtained from MicroSource. For retesting and post-screen analyses, individual compounds were obtained from Sigma-Aldrich and MicroSource.

C. elegans strains, maintenance and bleach-synchronization

Animals were cultured as previously described (63). All experiments were performed with the wild-type N2 strain of *Caenorhabditis elegans* unless otherwise indicated. The *smf-3(ok1035)* mutant strain RB1074 was obtained from the CGC. To generate bleach-synchronized L1 stage animals, L4 animals were first picked onto 10 cm NGM plates and grown for ~96 hours at 21ºC. Worms were then washed off plates with M9, and treated with ~4% NaClO / 1 M NaOH solution for 1 – 3 minutes to extract embryos, then washed with M9. Embryos were incubated in M9 for 18 – 24 hours at 21ºC to allow hatching.

N. parisii strains and spore preparation

Nematocida parisii spores were prepared as previously described (23). All experiments were performed with *N. parisii* strain ERTm1.

96-well plate-based screen for microsporidia inhibitors

C. elegans liquid culture methods and 96-well plate-based screening methods were partially adapted from established protocols (32, 64). *N. parisii* spores were prepared as described above, mixed in K-medium (51 mM NaCl, 32 mM KCl, 3 mM CaCl2, 3 mM MgSO4, 3.25 µM cholesterol) with 5x saturated OP50-1 *E. coli*, and added to 96-well culture plate. 96-well Spectrum Collection plates were thawed from –80ºC. Using a V&P Scientific 96-well pinning tool, 300 nL of DMSO-dissolved compounds were pinned into screening plate columns 2 – 11, and 300 nL of DMSO was pinned into screening plate columns 1 and 12 to be used for DMSO infected, DMSO uninfected, and fumagillin controls. Bleach-synchronized L1s were prepared as described above, mixed in K-medium with 5x saturated OP50-1 *E. coli*, and added to the screening plates. The final volume in each well was 50 µL, with ~100 L1s, *N.*

parisii spores at a final concentration of 6,250 spores/µL, DMSO at a final concentration of <1%, and compounds at a final concentration of 60 µM except for fumagillin (used at a concentration of 350 µM in all experiments). Screening plates were covered with adhesive porous film, placed in parafilm wrapped humidity boxes, and incubated at 21°C, shaking at 180 rpm for 6 days. After incubation, progeny production was scored visually. Initial hits were rescreened at a final concentration of 60 µM in the same manner using individual compounds resuspended in DMSO.

Semi-automated quantification of progeny production

Bleach-synchronized L1s were treated with compounds +/- *N. parisii* spores in 96-well plates prepared and incubated as described above. Three wells were assayed for each condition for each biological replicate. After incubation, animals were stained by adding 10 µL of 0.3125 mg/mL Rose Bengal solution to each well using an Integra VIAFLO 96 Electronic pipette. Plates were wrapped in parafilm and incubated at 37°C for 16 – 24 hours. To each well, 240 µL of M9+0.1% Tween-20 was added. Plates were then centrifuged for 1 minute at 2200 x g. Next, 200 µL was removed and 150 µL of M9+0.1% Tween-20 added to each well. 25 µL from each well was then transferred to a white 96-well plate containing 300 µL M9 per well. Plates were imaged using an Epson Perfection V850 Pro flat-bed scanner with the following parameters (dpi = 4800, colour = 24-bit, .jpg compression = 1). Images were edited in GIMP version 2.10 or later to highlight stained animals by removing HTML colour codes #000000 and #FFC9AF, applying unsharp masking with the following parameters (radius = 10, effect = 10, threshold = 10), editing hue saturation with the following parameters (For yellow, green, blue and cyan: lightness = 100, saturation = -100. For red and magenta: lightness = -100, saturation = 100), and exporting each well as a single .tiff image with LZW compression (65). The number of animals in each well was counted using the MATLAB-based phenotypic analysis tool WorMachine with the following parameters (pixel neighbouring threshold = 1, pixel binarization threshold = 30, max object area to remove = 0.003%) (39).

Continuous infection assays

Continuous infection assays were performed in 24-well assay plates with each well containing a final volume 400 µL, ~800 L1s, 5,000 *N. parisii* spores/µL, 60 µM of each compound except for fumagillin (see above), and DMSO at a final concentration of 1%. Three wells were assayed for each compound for each of three biological replicates. Assay plates were covered with adhesive porous film, placed in parafilm wrapped humidity boxes, incubated at 21ºC, 180 rpm for 4 days, and stored at 4ºC, 20 rpm for 1 – 2 days. After incubation, samples were acetone-fixed, DY96-stained, and subject to fluorescence microscopy as described below.

Pulse infection assays

~8,000 bleach-synchronized L1s and 10 million *N. parisii* spores were added to 6 cm NGM plates with 10 µL 10x OP50-1. Plates were dried in a clean cabinet and incubated for a total of 3 hours at room temperature. After pulse infection, animals were washed 1 – 2x with 1 mL M9+0.1% Tween-20 to remove excess spores, then added to transparent 24-well assay plates prepared as described above for the continuous infection assay, except without adding any spores. Three wells were assayed for each compound for each of three biological replicates. Assay plates were treated as described for continuous infection assays, except the incubation period was either 2 or 4 days. Samples incubated for 4 days were acetone-fixed, FISH-stained and DY96-stained, while samples incubated for 2 days were fixed in 4% PFA and FISH-stained. Fluorescence microscopy was performed as described below.

Spore firing assays

24-well assay plates were prepared exactly as in the continuous infection assay with *N. parisii* spores at a final concentration of 5,000 spores/µL, compounds at a final concentration of 60 µM except for fumagillin (see above), and DMSO at a final concentration of 1%. For all spore firing assays containing TPCK, spores at a concentration of 10,000 spores/µL were incubated for 24 hours at 21ºC in K-medium with compounds at a concentration of 120 µM, and DMSO at a concentration of 2%. These spores were then used to prepare assay plates exactly as in the continuous infection assay with final concentrations as stated above. For all spore firing assays where excess compound was removed prior to infection,

spores were washed 3x with 1 mL K-medium before being used in assay plate preparation. Three wells were assayed for each compound for each of three biological replicates. Assay plates were covered with adhesive porous film, placed in parafilm wrapped humidity boxes, and incubated at 21ºC, shaking at 180 rpm for 3 hours. After incubation, samples were acetone-fixed, FISH-stained, DY96-stained, and subject to fluorescence microscopy as described below.

Iron chelation and supplementation

24-well assay plates were prepared exactly as in the continuous infection assay with *N. parisii* spores at a final concentration of 5,000 spores/µL (normal dose) or 78 spores/µL (low dose), 2,2'-bipyridyl (BP) or dexrazoxane at a final concentration of 60 µM, water-dissolved ferric ammonium citrate (FAC) at a final concentration of 6.6 mg/mL, and DMSO at a final concentration of 1%. Assay plates were treated as described for continuous infection assays. After incubation, samples were acetone-fixed, DY96-stained, and subject to fluorescence microscopy as described below.

RB1074 drug sensitivity tests

~1000 RB1074 or N2 bleach-synchronized L1s were added to 6 cm NGM plates top plated with 120 µL 10x OP50-1, 2,2'-bipyridyl (BP) or dexrazoxane at a final concentration of 60 µM, and DMSO at a final concentration of 1%. Plates were dried in a clean cabinet for ~1 hour at room temperature, and then incubated at 21ºC for 3 days. After incubation, live animals were imaged using a Leica Microsystems dissecting scope.

DY96 staining, fluorescence in situ hybridization (FISH), and microscopy

Post-incubation, samples were washed 1 – 2x with 1 mL M9+0.1% Tween-20 to remove excess OP50, fixed in 700 µL acetone and stored at –20ºC, or fixed in 500 µL PFA solution (4% PFA, 1x PBS, 0.1% Tween-20) and stored at 4ºC until ready for subsequent steps. Samples were then washed 1 – 2x with 1 mL 1xPBS+0.1% Tween-20 and 1x with 1 mL hybridization buffer (900 mM NaCl, 20 mM Tris HCl, 0.01% SDS). 100 µL FISH staining solution (5 ng/µL *N. parisii* 18S RNA-specific microB red FISH

probe in hybridization buffer) (27) was added, and samples were incubated for 18 – 24 hours at 46°C. After FISH incubation, samples were washed 1x with 1 mL wash buffer (50 mL hybridization buffer + 5 mM EDTA) to remove excess FISH probes. 500 µL DY96 staining solution (20 ug/uL DY96, 0.1% SDS in 1xPBS+0.1% Tween-20) was added, and samples were incubated for 1 hour at 21°C. After DY96 incubation, samples were suspended in EverBrite™ Mounting Medium with DAPI, and subject to fluorescence microscopy using a ZEISS Axio Imager 2 at 5x – 63x magnification. For continuous infection assays, FISH staining steps were omitted, and just stained with DY96.

Quantification of FISH fluorescence

FISH fluorescence was quantified using FIJI (66). Animal area was determined by outlining boundaries based on DAPI staining. Minimum fluorescence threshold for FISH signal was set to 4000 to exclude auto-fluorescence and background staining of embryos while maximizing inclusion of FISH-stained *N. parisii* sporoplasms and meronts. The percentage area of animal covered by FISH signal was calculated.

Statistical analysis

All statistical analyses were conducting using Microsoft Excel and R version 3.6.1 or later accessed via RStudio version 1.2.5019 or later (67–69).

References

1. Murareanu BM, Sukhdeo R, Qu R, Jiang J, Reinke AW. Generation of a Microsporidia Species Attribute Database and Analysis of the Extensive Ecological and Phenotypic Diversity of Microsporidia. mBio 12:e01490-21.

2. Wadi L, Reinke AW. 2020. Evolution of microsporidia: An extremely successful group of eukaryotic intracellular parasites. PLoS Pathog 16:e1008276.

428 3. Stentiford GD, Feist SW, Stone DM, Bateman KS, Dunn AM. 2013. Microsporidia: diverse, dynamic, and
429 emergent pathogens in aquatic systems. Trends Parasitol 29:567–578.

430 4. Burnham AJ. 2019. Scientific Advances in Controlling Nosema ceranae (Microsporidia) Infections in Honey
431 Bees (Apis mellifera). Front Vet Sci 6.

432 5. Chaijarasphong T, Munkongwongsiri N, Stentiford GD, Aldama-Cano DJ, Thansa K, Flegel TW,
433 Sritunyalucksana K, Itsathitphaisarn O. 2020. The shrimp microsporidian Enterocytozoon hepatopenaei
434 (EHP): Biology, pathology, diagnostics and control. Journal of Invertebrate Pathology 107458.

435 6. Ding Z, Meng Q, Liu H, Yuan S, Zhang F, Sun M, Zhao Y, Shen M, Zhou G, Pan J, Xue H, Wang W. 2016. First
436 case of hepatopancreatic necrosis disease in pond-reared Chinese mitten crab, Eriocheir sinensis,
437 associated with microsporidian. Journal of Fish Diseases 39:1043–1051.

438 7. Bhat IA, Buhroo Z, Bhat MA. 2017. Microsporidiosis in silkworms with particular reference to mulberry
439 silkworm (Bombyx Mori L.). International Journal of Entomology Research 2:01–09.

440 8. Picard-Sánchez A, Piazzon MC, Ahmed NH, Del Pozo R, Sitjà-Bobadilla A, Palenzuela O. 2020. Enterospora
441 nucleophila (Microsporidia) in Gilthead Sea Bream (Sparus aurata): Pathological Effects and Cellular
442 Immune Response in Natural Infections. Vet Pathol 57:565–576.

443 9. Kent ML, Elliott DG, Groff JM, Hedrick RP. 1989. Loma salmonae (Protozoa: Microspora) infections in
444 seawater reared coho salmon Oncorhynchus kisutch. Aquaculture 80:211–222.

445 10. Shinn A, Pratoomyot J, Griffiths D, Trọng T, Thanh Vu N, Jiravanichpaisal P, Briggs M. 2018. Asian Shrimp
446 Production and the Economic Costs of Disease. Asian Fisheries Science 31S.

447 11. Ruan Y, Xu X, He Q, Li L, Guo J, Bao J, Pan G, Li T, Zhou Z. 2021. The largest meta-analysis on the global
448 prevalence of microsporidia in mammals, avian and water provides insights into the epidemic features of
449 these ubiquitous pathogens. Parasites & Vectors 14:186.

450 12. Ostroverkhova NV, Konusova OL, Kucher AN, Kireeva TN, Rosseykina SA. 2020. Prevalence of the
451 Microsporidian Nosema spp. in Honey Bee Populations (Apis mellifera) in Some Ecological Regions of North
452 Asia. 3. Veterinary Sciences 7:111.

453 13. Stentiford GD, Becnel JJ, Weiss LM, Keeling PJ, Didier ES, Williams BAP, Bjornson S, Kent ML, Freeman MA,
454 Brown MJF, Troemel ER, Roesel K, Sokolova Y, Snowden KF, Solter L. 2016. Microsporidia – Emergent
455 Pathogens in the Global Food Chain. Trends Parasitol 32:336–348.

456 14. Katznelson H, Jamieson CA. 1952. Control of Nosema Disease of Honeybees with Fumagillin. Science
457 115:70–71.

458 15. Huang W-F, Solter LF, Yau PM, Imai BS. 2013. Nosema ceranae Escapes Fumagillin Control in Honey Bees.
459 PLOS Pathogens 9:e1003185.

460 16. Tang KFJ, Han JE, Aranguren LF, White-Noble B, Schmidt MM, Piamsomboon P, Risdiana E, Hanggono B.
461 2016. Dense populations of the microsporidian Enterocytozoon hepatopenaei (EHP) in feces of Penaeus
462 vannamei exhibiting white feces syndrome and pathways of their transmission to healthy shrimp. Journal
463 of Invertebrate Pathology 140:1–7.

464 17. van den Heever JP, Thompson TS, Curtis JM, Ibrahim A, Pernal SF. 2014. Fumagillin: an overview of recent
465 scientific advances and their significance for apiculture. J Agric Food Chem 62:2728–2737.

466 18. Han B, Weiss LM. 2018. Therapeutic targets for the treatment of microsporidiosis in humans. Expert Opin
467 Ther Targets 22:903–915.

468 19. He Q, Leitch GJ, Visvesvara GS, Wallace S. 1996. Effects of nifedipine, metronidazole, and nitric oxide
469 donors on spore germination and cell culture infection of the microsporidia Encephalitozoon hellem and
470 Encephalitozoon intestinalis. Antimicrob Agents Chemother 40:179–185.

471 20. Didier ES, Maddry JA, Kwong CD, Green LC, Snowden KF, Shadduck JA. 1998. Screening of compounds for
472 antimicrosporidial activity in vitro. Folia Parasitologica 45:129–139.

473 21. Borges D, Guzman-Novoa E, Goodwin PH. 2020. Control of the microsporidian parasite Nosema ceranae in
474 honey bees (Apis mellifera) using nutraceutical and immuno-stimulatory compounds. PLOS ONE
475 15:e0227484.

476 22. Zhang G, Sachse M, Prevost M-C, Luallen RJ, Troemel ER, Felix M-A. 2016. A Large Collection of Novel
477 Nematode-Infecting Microsporidia and Their Diverse Interactions with Caenorhabditis elegans and Other
478 Related Nematodes. PLoS Pathog 12:e1006093.

479 23. Willis AR, Zhao W, Sukhdeo R, Wadi L, Jarkass HTE, Claycomb JM, Reinke AW. 2021. A parental
480 transcriptional response to microsporidia infection induces inherited immunity in offspring. Science
481 Advances 7:eabf3114.

482 24. Bakowski MA, Desjardins CA, Smelkinson MG, Dunbar TL, Lopez-Moyado IF, Rifkin SA, Cuomo CA, Troemel
483 ER. 2014. Ubiquitin-mediated response to microsporidia and virus infection in C. elegans. PLoS Pathog
484 10:e1004200.

485 25. Reinke AW, Balla KM, Bennett EJ, Troemel ER. 2017. Identification of microsporidia host-exposed proteins
486 reveals a repertoire of rapidly evolving proteins. Nat Commun 8:14023.

487 26. Estes KA, Szumowski SC, Troemel ER. 2011. Non-lytic, actin-based exit of intracellular parasites from C.
488 elegans intestinal cells. PLoS Pathog 7:e1002227.

489 27. Troemel ER, Félix M-A, Whiteman NK, Barrière A, Ausubel FM. 2008. Microsporidia Are Natural
490 Intracellular Parasites of the Nematode Caenorhabditis elegans. PLOS Biology 6:e309.

491 28. Balla KM, Luallen RJ, Bakowski MA, Troemel ER. 2016. Cell-to-cell spread of microsporidia causes
492 Caenorhabditis elegans organs to form syncytia. 11. Nature Microbiology 1:1–6.

493 29. Luallen RJ, Reinke AW, Tong L, Botts MR, Felix M-A, Troemel ER. 2016. Discovery of a Natural
494 Microsporidian Pathogen with a Broad Tissue Tropism in Caenorhabditis elegans. PLoS Pathog
495 12:e1005724.

496 30. Ewbank JJ, Zugasti O. 2011. C. elegans: model host and tool for antimicrobial drug discovery. Disease
497 Models & Mechanisms 4:300–304.

498 31. Peterson ND, Pukkila-Worley R. 2018. C. elegans in high-throughput screens for anti-infective compounds.
499 Curr Opin Immunol 54:59–65.

500 32. Burns AR, Luciani GM, Musso G, Bagg R, Yeo M, Zhang Y, Rajendran L, Glavin J, Hunter R, Redman E, Stasiuk
501 S, Schertzberg M, Angus McQuibban G, Caffrey CR, Cutler SR, Tyers M, Giaever G, Nislow C, Fraser AG,
502 MacRae CA, Gilleard J, Roy PJ. 2015. Caenorhabditis elegans is a useful model for anthelmintic discovery. 1.
503 Nature Communications 6:7485.

504 33. Anastassopoulou CG, Fuchs BB, Mylonakis E. 2011. Caenorhabditis elegans-based Model Systems for
505 Antifungal Drug Discovery. Curr Pharm Des 17:1225–1233.

506 34. Mylonakis E, Ausubel FM, Perfect JR, Heitman J, Calderwood SB. 2002. Killing of Caenorhabditis elegans by
507 Cryptococcus neoformans as a model of yeast pathogenesis. Proc Natl Acad Sci U S A 99:15675–15680.

508 35. Moy TI, Ball AR, Anklesaria Z, Casadei G, Lewis K, Ausubel FM. 2006. Identification of novel antimicrobials
509 using a live-animal infection model. Proc Natl Acad Sci U S A 103:10414–10419.

510 36. Moy TI, Conery AL, Larkins-Ford J, Wu G, Mazitschek R, Casadei G, Lewis K, Carpenter AE, Ausubel FM.
511 2009. High-throughput screen for novel antimicrobials using a whole animal infection model. ACS Chem
512 Biol 4:527–533.

513 37. O'Reilly LP, Luke CJ, Perlmutter DH, Silverman GA, Pak SC. 2014. C. elegans in high-throughput drug
514 discovery. Adv Drug Deliv Rev 0:247–253.

515 38. Luallen RJ, Bakowski MA, Troemel ER. 2015. Characterization of Microsporidia-Induced Developmental
516 Arrest and a Transmembrane Leucine-Rich Repeat Protein in Caenorhabditis elegans. PLOS ONE
517 10:e0124065.

518 39. Hakim A, Mor Y, Toker IA, Levine A, Neuhof M, Markovitz Y, Rechavi O. 2018. WorMachine: machine
519 learning-based phenotypic analysis tool for worms. BMC Biology 16:8.

520 40. Wittkowski P, Violet N, Oelgeschläger M, Schönfelder G, Vogl S. 2020. A quantitative medium-throughput
521 assay to measure Caenorhabditis elegans development and reproduction. STAR Protocols 1:100224.

522 41. Wittkowski P, Marx-Stoelting P, Violet N, Fetz V, Schwarz F, Oelgeschläger M, Schönfelder G, Vogl S. 2019.
523 Caenorhabditis elegans As a Promising Alternative Model for Environmental Chemical Mixture Effect
524 Assessment—A Comparative Study. Environ Sci Technol 53:12725–12733.

525 42. Mathew MD, Mathew ND, Ebert PR. 2012. WormScan: A Technique for High-Throughput Phenotypic
526 Analysis of Caenorhabditis elegans. PLOS ONE 7:e33483.

527 43. Vávra J, Larsson JIR. 2014. Structure of Microsporidia, p. 1–70. *In* Microsporidia. John Wiley & Sons, Ltd.

528 44. Zhang G, Sachse M, Prevost M-C, Luallen RJ, Troemel ER, Félix M-A. 2016. A Large Collection of Novel
529 Nematode-Infecting Microsporidia and Their Diverse Interactions with Caenorhabditis elegans and Other
530 Related Nematodes. PLOS Pathogens 12:e1006093.

531 45. Rodríguez-García C, Heerman MC, Cook SC, Evans JD, DeGrandi-Hoffman G, Banmeke O, Zhang Y, Huang S,
532 Hamilton M, Chen YP. 2021. Transferrin-mediated iron sequestration suggests a novel therapeutic strategy
533 for controlling Nosema disease in the honey bee, Apis mellifera. PLoS Pathogens 17.

534 46. Didier ES, Bowers LC, Martin AD, Kuroda MJ, Khan IA, Didier PJ. 2010. Reactive nitrogen and oxygen
535 species, and iron sequestration contribute to macrophage-mediated control of Encephalitozoon cuniculi
536 (Phylum Microsporidia) infection in vitro and in vivo. Microbes and Infection 12:1244–1251.

537 47. Rajan M, Anderson CP, Rindler PM, Romney SJ, Ferreira dos Santos MC, Gertz J, Leibold EA. 2019. NHR-14
538 loss of function couples intestinal iron uptake with innate immunity in C. elegans through PQM-1 signaling.
539 eLife 8:e44674.

540 48. Tamim El Jarkass H, Mok C, Schertzberg MR, Fraser AG, Troemel ER, Reinke AW. 2021. An intestinally
541 secreted host factor limits bacterial colonization but promotes microsporidia invasion of C. elegans. bioRxiv
542 2021.07.12.452088.

543 49. Dang X, Pan G, Li T, Lin L, Ma Q, Geng L, He Y, Zhou Z. 2013. Characterization of a subtilisin-like protease
544 with apical localization from microsporidian Nosema bombycis. J Invertebr Pathol 112:166–174.

545 50. Yavelow J, Caggana M, Beck KA. 1987. Proteases occurring in the cell membrane: a possible cell receptor
546 for the Bowman-Birk type of protease inhibitors. Cancer Res 47:1598–1601.

547 51. Reichardt P, Tabone M-D, Mora J, Morland B, Jones RL. 2018. Risk–benefit of dexrazoxane for preventing
548 anthracycline-related cardiotoxicity: re-evaluating the European labeling. Future Oncology 14:2663–2676.

549 52. Jones RL. 2008. Utility of dexrazoxane for the reduction of anthracycline-induced cardiotoxicity. Expert
550 Review of Cardiovascular Therapy 6:1311–1317.

551 53. Hasinoff BB. 1998. Chemistry of dexrazoxane and analogues. Semin Oncol 25:3–9.

552 54. Kirienko NV, Kirienko DR, Larkins-Ford J, Wählby C, Ruvkun G, Ausubel FM. 2013. Pseudomonas aeruginosa
553 Disrupts Caenorhabditis elegans Iron Homeostasis, Causing a Hypoxic Response and Death. Cell Host &
554 Microbe 13:406–416.

555 55. Deng S, Yan T, Nikolova T, Fuhrmann D, Nemecek A, Gödtel-Armbrust U, Kaina B, Wojnowski L. 2015. The
556 catalytic topoisomerase II inhibitor dexrazoxane induces DNA breaks, ATF3 and the DNA damage response
557 in cancer cells. British Journal of Pharmacology 172:2246–2257.

558 56. Zdraljevic S, Strand C, Seidel HS, Cook DE, Doench JG, Andersen EC. 2017. Natural variation in a single
559 amino acid substitution underlies physiological responses to topoisomerase II poisons. PLOS Genetics
560 13:e1006891.

561 57. Han B, Takvorian PM, Weiss LM. 2020. Invasion of Host Cells by Microsporidia. Front Microbiol 11.

562 58. Tamim El Jarkass H, Reinke AW. 2020. The ins and outs of host-microsporidia interactions during invasion,
563 proliferation and exit. Cellular Microbiology 22:e13247.

564 59. Dang X, Pan G, Li T, Lin L, Ma Q, Geng L, He Y, Zhou Z. 2013. Characterization of a subtilisin-like protease
565 with apical localization from microsporidian Nosema bombycis. J Invertebr Pathol 112:166–174.

566 60. P. Wilson BA, C. Thornburg C, J. Henrich C, Grkovic T, R. O'Keefe B. 2020. Creating and screening natural
567 product libraries. Natural Product Reports 37:893–918.

568 61. Rosenberg A, Luth MR, Winzeler EA, Behnke M, Sibley LD. 2019. Evolution of resistance in vitro reveals
569 mechanisms of artemisinin activity in Toxoplasma gondii. PNAS 116:26881–26891.

570 62. Cowell AN, Istvan ES, Lukens AK, Gomez-Lorenzo MG, Vanaerschot M, Sakata-Kato T, Flannery EL,
571 Magistrado P, Owen E, Abraham M, LaMonte G, Painter HJ, Williams RM, Franco V, Linares M, Arriaga I,
572 Bopp S, Corey VC, Gnädig NF, Coburn-Flynn O, Reimer C, Gupta P, Murithi JM, Moura PA, Fuchs O, Sasaki E,
573 Kim SW, Teng CH, Wang LT, Akidil A, Adjalley S, Willis PA, Siegel D, Tanaseichuk O, Zhong Y, Zhou Y, Llinás
574 M, Ottilie S, Gamo F-J, Lee MCS, Goldberg DE, Fidock DA, Wirth DF, Winzeler EA. 2018. Mapping the
575 malaria parasite druggable genome by using in vitro evolution and chemogenomics. Science 359:191–199.

576 63. Lewis JA, Fleming JT. 1995. Basic culture methods. Methods Cell Biol 48:3–29.

577 64. Lehner B, Tischler J, Fraser AG. 2006. RNAi screens in Caenorhabditis elegans in a 96-well liquid format and
578 their application to the systematic identification of genetic interactions. 3. Nature Protocols 1:1617–1620.

65. The GIMP Development Team. 2018. GIMP. https://www.gimp.org.

66. Schindelin J, Arganda-Carreras I, Frise E, Kaynig V, Longair M, Pietzsch T, Preibisch S, Rueden C, Saalfeld S, Schmid B, Tinevez J-Y, White DJ, Hartenstein V, Eliceiri K, Tomancak P, Cardona A. 2012. Fiji: an open-source platform for biological-image analysis. Nat Methods 9:676–682.

67. Microsoft Corporation. 2021. Microsoft Excel. https://office.microsoft.com/excel.

68. R Core Tam. 2021. R: A language and environment for statistical computing. https://wwwR-project.org.

69. RStudio Team. 2020. RStudio: Integrated Development for R. https://rstudio.com.

Figures and Tables

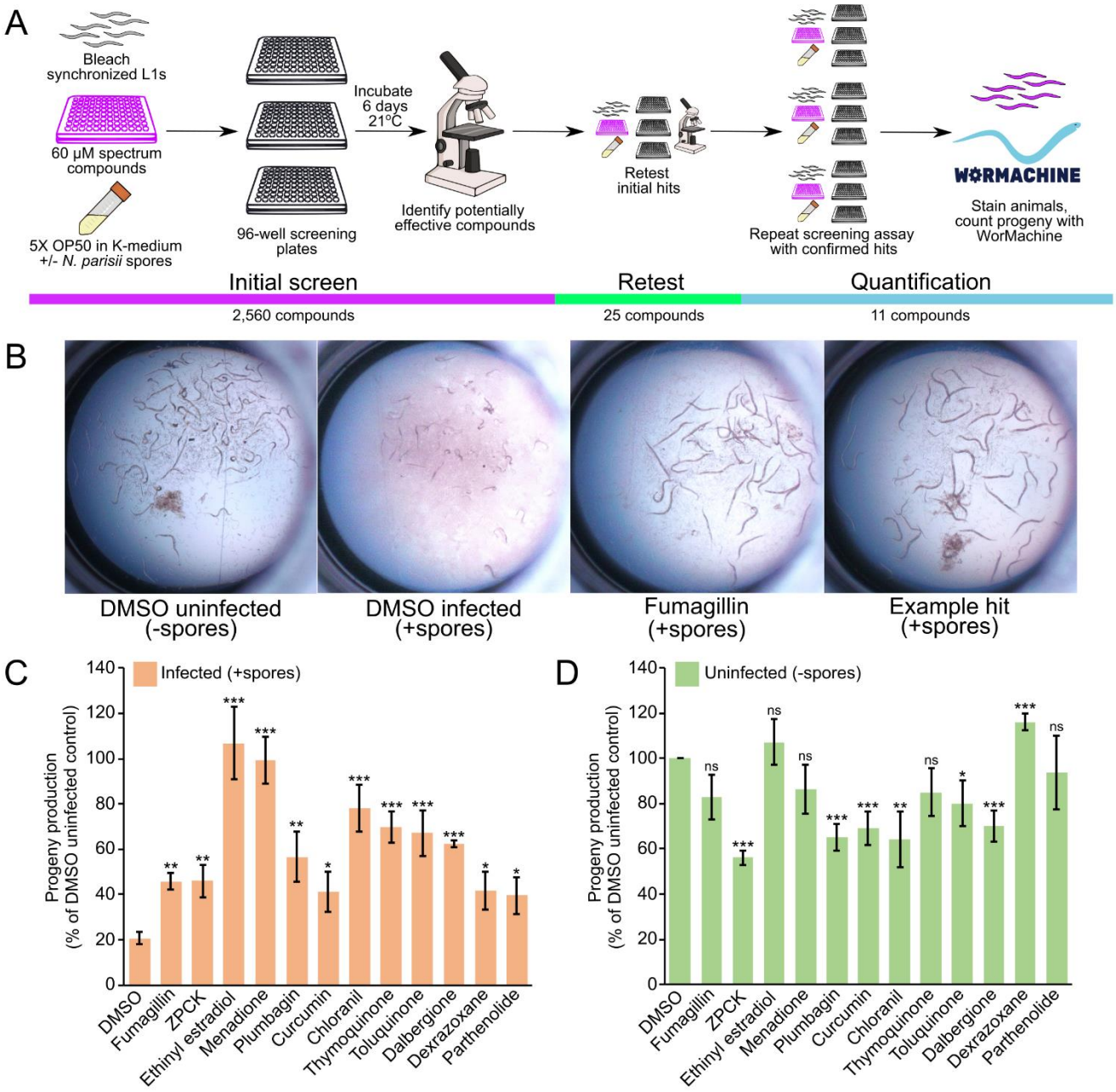

Figure 1. High-throughput drug screen of the Spectrum Collection identifies compounds that restore progeny production in *C. elegans* infected with *N. parisii*. (A) Schematic of small molecule inhibitor screen (see methods). Bleach-synchronized L1 animals were incubated with 60 µM of each compound from the Spectrum Collection for 6 days at 21 °C in the presence of *N. parisii* spores. 2,560 total compounds were screened once, yielding 25 initial hits. The initial hits were retested once, yielding 11 confirmed hits. The effectiveness of these 11 compounds was then quantified across multiple replicates of the screening assay using WorMachine. **(B)** Representative images of wells containing

worms. **(B Far Left)** Normal worm growth in the absence of spores. **(B Middle Left)** Microsporidia infection leads to inhibition of progeny production. **(B Middle & Far Right)** Treatment with anti-microsporidial compounds restores progeny production. **(C & D)** Effect of compounds on progeny production in **(C)** infected and **(D)** uninfected animals. Progeny levels expressed as a percentage of the DMSO uninfected control. Statistical significance evaluated in relation to DMSO controls using t-tests: *** = $p < 0.001$, ** = $p < 0.01$, * = $p < 0.05$, *ns = not significant* ($p > 0.05$). Data for each condition includes 3 – 6 biological replicates.

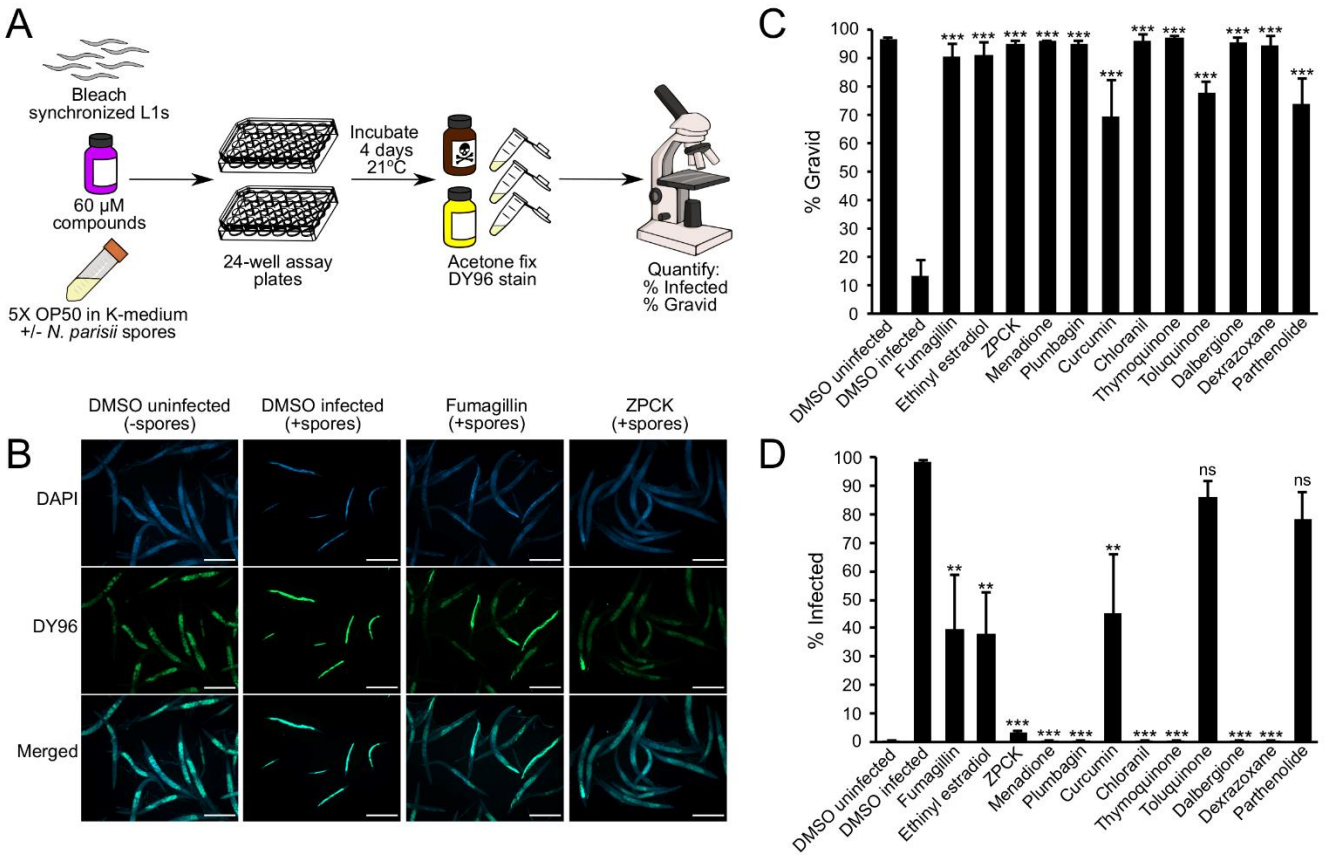

Figure 2. Identified compounds inhibit microsporidia infection. (A) Schematic of continuous infection assay (see methods). Bleach-synchronized L1 animals were incubated with compounds for 4 days at 21 °C in the presence of *N. parisii* spores in liquid. Animals were subsequently fixed with acetone, and stained with DAPI and DY96. **(B)** Representative images taken at 5x magnification; scale bars are 500 µm. **(B Far Left)** Normal worm growth in the absence of spores. **(B Middle Left)** Microsporidia infection results in production of new spores highlighted in bright green by DY96, and

slows growth thereby preventing development of gravid adults. **(B Middle Right & Far Right)** Treatment with anti-microsporidial compounds reduces formation of new spores, and restores the development of gravid adults. **(C)** Percentage of animals that contain embryos (N = ≥200 animals counted per biological replicate). **(D)** Percentage of animals that contain newly formed spores (N = ≥200 animals counted per biological replicate). Significance evaluated in relation to DMSO infected controls using one-way ANOVA with Dunnett's post-hoc test: *** = $p < 0.001$, ** = $p < 0.01$, * = $p < 0.05$, *ns* = *not significant* ($p > 0.05$). Data for each condition includes 3 biological replicates.

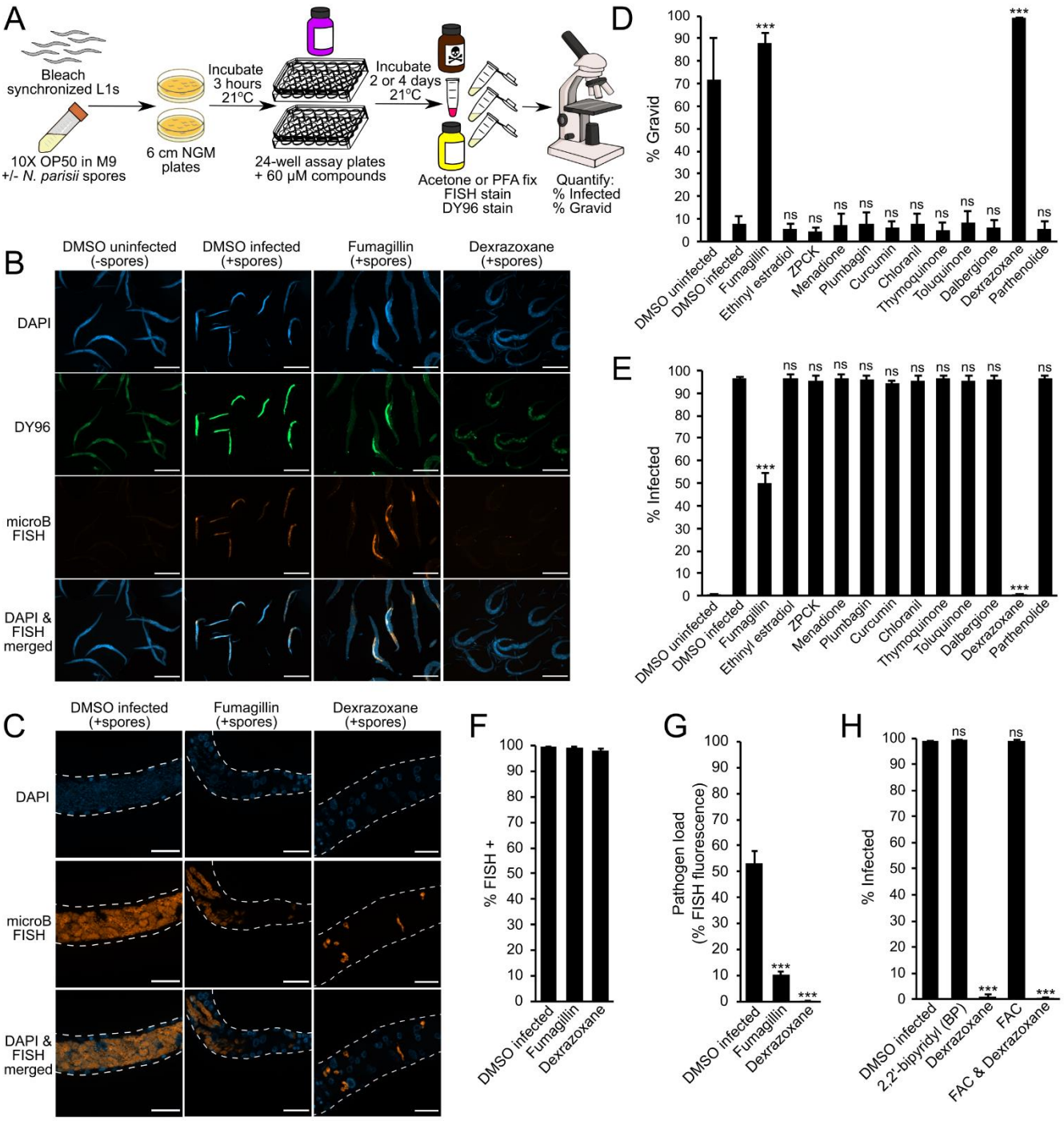

Figure 3. Dexrazoxane prevents microsporidia proliferation. (A) Schematic of pulse-chase infection assay (see methods). Bleach-synchronized L1 animals were pulse infected with *N. parisii* spores for 3 hours at 21 °C on NGM plates. Excess spores were washed away, and infected animals were incubated with compounds for 2 or 4 days at 21 °C in liquid. Animals were fixed in acetone or PFA, FISH stained, and then stained with DY96 and DAPI. **(B)** Representative images of acetone-fixed animals 4 days post infection taken at 5x magnification; scale bars are 500 µm. **(B Far Left)** Normal

growth in uninfected worms. **(B Middle Left)** Pulse infection results in sporoplasms and meronts highlighted in red by microB FISH probes and new spores highlighted in bright green by DY96. Pulse infection also slows growth thereby preventing development of gravid adults. **(B Middle Right & Far Right)** Treatment of pulse-infected animals with fumagillin or dexrazoxane reduces sporoplasms and meronts, new spores, and restores development of gravid adults. **(C)** Representative images (z-stack maximum intensity projections; 7 slices, 0.25 µm spacing) of PFA-fixed animals 2 days post infection taken at 63x magnification; scale bars are 20 µm. **(C Left)** In the absence of drug treatment, pulse-infected animals develop large meronts with many nuclei. **(C Middle)** Fumagillin treatment restricts proliferation; both large and small meronts are observed. **(C Right)** Dexrazoxane treatment restricts proliferation; only small meronts with one or two nuclei are observed. **(D)** Percentage of animals with embryos (N = ≥170 animals counted per biological replicate). **(E)** Percentage of animals with newly formed spores (N = ≥170 animals counted per biological replicate). **(F)** Percentage of animals with FISH signal (N = ≥170 animals counted per biological replicate). ANOVA not significant ($p = 0.111$). **(G)** Quantitation of FISH fluorescence per worm (N = 15 animals quantified per biological replicate). **(H)** Effects of iron chelation with BP on infection, and effects of iron supplementation with FAC on dexrazoxane activity. Percentage of animals with newly formed spores (N = ≥120 animals counted per biological replicate) after 4 days of continuous infection is shown. Significance evaluated in relation to DMSO infected controls using one-way ANOVA with Dunnett's post-hoc test: *** = $p < 0.001$, ** = $p < 0.01$, * = $p < 0.05$, *ns = not significant* ($p > 0.05$). Data for each condition includes 3 biological replicates.

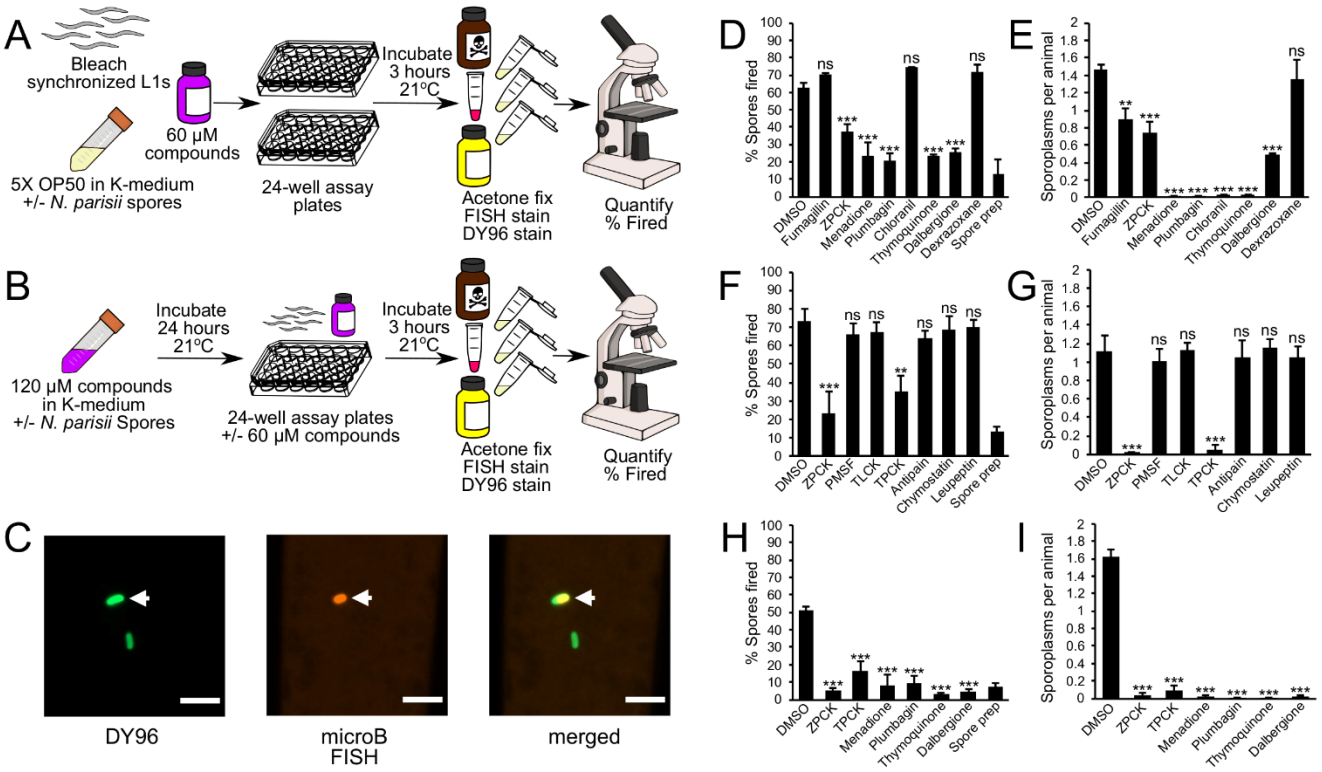

Figure 4. Several compounds prevent microsporidia infection by inhibiting spore firing. (A) Schematic of spore firing assay (see methods). Bleach-synchronized L1 animals were incubated with compounds for 3 hours at 21 °C in the presence of *N. parisii* spores in liquid. Spore prep control was generated by incubating spores in liquid in the absence of *C. elegans*. Animals and spores were fixed in acetone, and stained with microB FISH probes and DY96. **(B)** Schematic of modified spore firing assay (see methods). Spores were incubated with compounds for 24 hours at 21 °C**,** and then used to infect beach-synchronized L1 animals either with or without prior washing to remove excess compounds. **(C)** Representative images of unfired and fired spores at 63x magnification; scale bars are 5 µm. Unfired spore is indicated by white arrowhead. **(D & E)** Effects of microsporidia inhibitors on **(D)** the percentage of fired spores in the *C. elegans* intestinal lumen (N = ≥60 spores counted per biological replicate) and **(E)** the average number of sporoplasms per animal (N = ≥40 animals counted per biological replicate) in a spore firing assay. **(F & G)** Effects of serine protease inhibitors on **(F)** spore firing and **(G)** sporoplasm invasion in a modified spore firing assay without washing away compounds prior to infection (N = ≥39 animals and ≥60 spores counted per biological replicate, except for one chymostatin replicate where only 12 animals and 19 spores were counted). **(H & I)** Effects of spore firing inhibitors

on **(H)** spore firing and **(I)** sporoplasm invasion in a modified spore firing assay with compounds washed away prior to infection (N = ≥40 animals and ≥70 spores counted per biological replicate). Significance evaluated in relation to DMSO controls using one-way ANOVA with Dunnett's post-hoc test: *** = *p < 0.001*, ** = *p < 0.01*, * = *p < 0.05*, *ns = not significant (p > 0.05)*. Data for each condition includes 3 biological replicates.

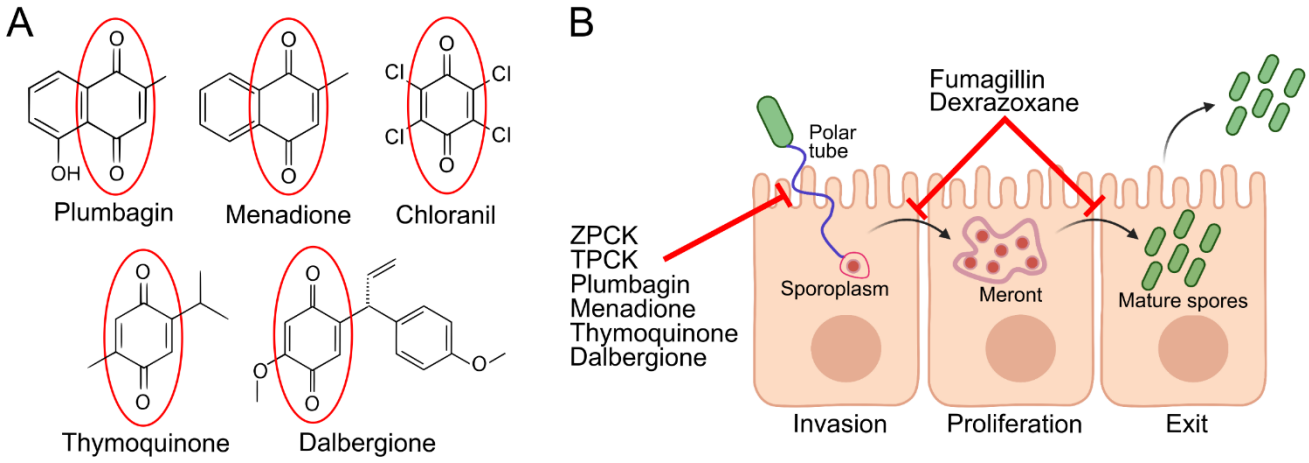

Figure 5. Compound structures and mechanisms. (A) Structures of compounds containing a quinone moiety (circled in red) that were identified in the initial screen as inhibitors of microsporidia infection. **(B)** Microsporidia infection model depicting the stages at which various microsporidia inhibitors act. Two protease inhibitors and four quinone-derivatives were shown to act directly on *N. parisii* spores to prevent spore firing and subsequent invasion of sporoplasms. Fumagillin and dexrazoxane act after invasion has occurred, inhibiting proliferation of sporoplasms and meronts, ultimately reducing parasite burden and preventing the production of microsporidia spores. Figure made using Biorender.com.

Supplemental material

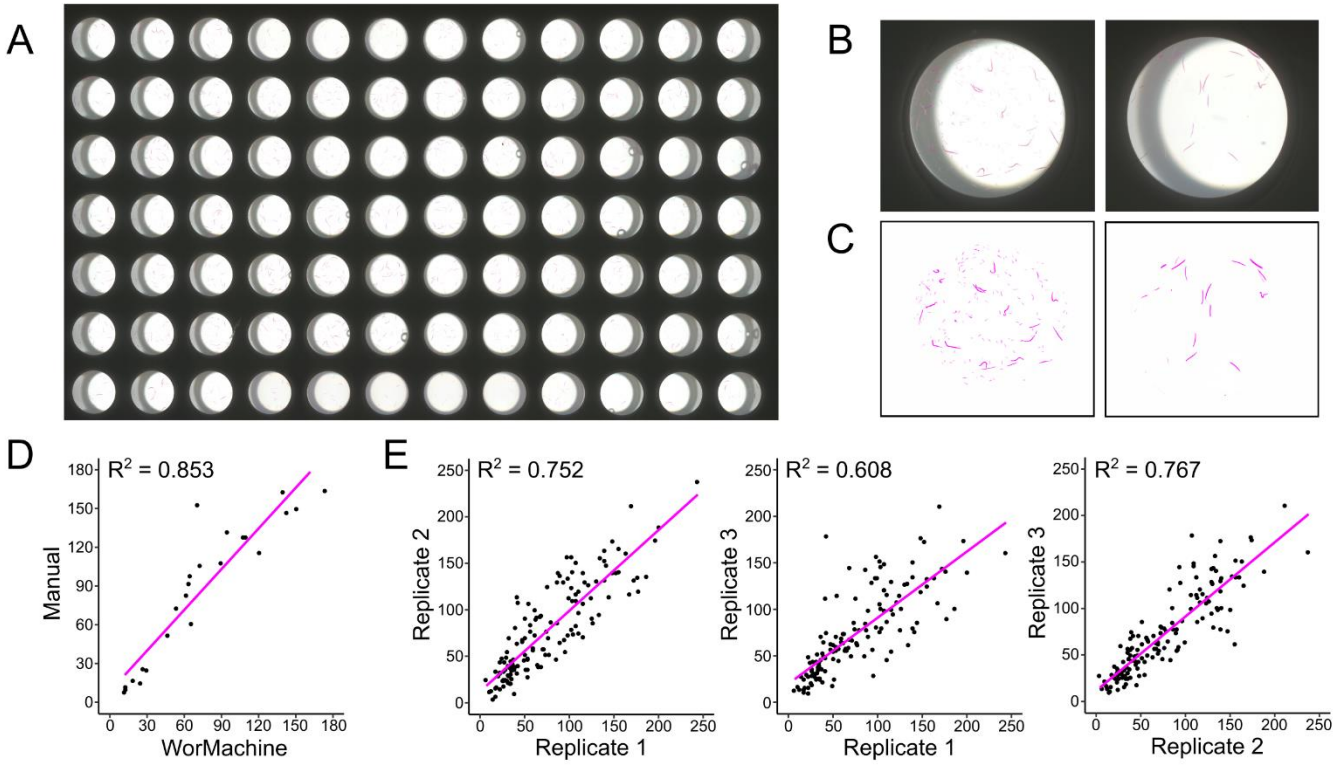

Figure S1. Quantitation of progeny number using semi-automated image processing. (A) Flatbed scanner image of a plate following staining and dilution steps. **(B)** Sample images of wells prior to processing. **(C)** Sample images of wells after processing. **(D)** Correlation between manual counts and WorMachine counts (N = 24). **(E)** Correlations between pairs of technical replicates as a measure of technical variability (N = 140 per correlation).

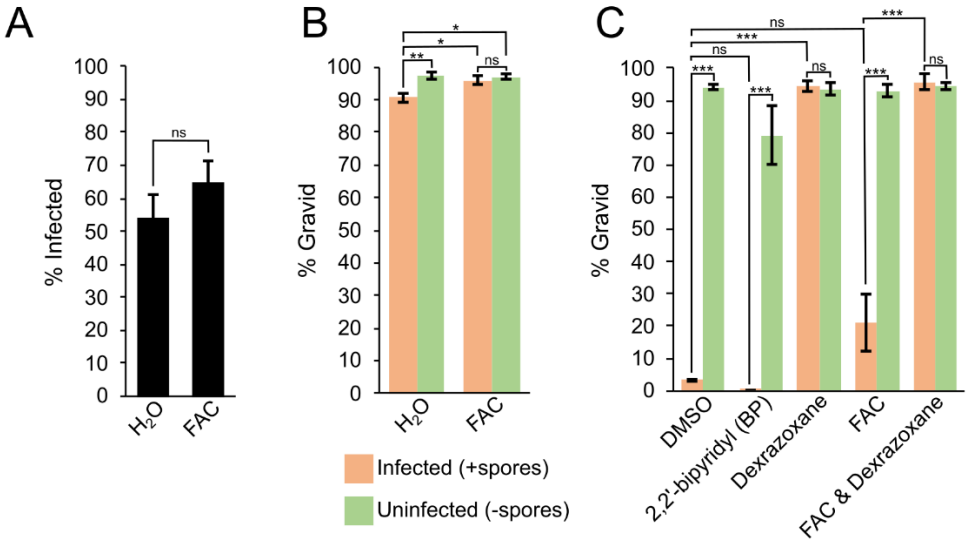

Figure S2. *N. parisii* infection in *C. elegans* is unaffected by altering iron levels. (A & B) Effects of iron supplementation with FAC on *N. parisii* infection in *C. elegans*. **(A)** Percentage of animals with newly formed spores (N = ≥140 animals counted per biological replicate; significance evaluated using a two-sample t-test) and **(B)** percentage of animals with embryos (N = ≥140 animals counted per biological replicate; significance evaluated using a one-way ANOVA with Tukey's post-hoc test) after 4 days of continuous infection with a low dose of spores are shown. **(C)** Effects of iron chelation with BP on infection, and effects of iron supplementation with FAC on dexrazoxane activity. Percentage of animals with embryos (N = ≥120 animals counted per biological replicate; significance evaluated using a one-way ANOVA with Tukey's post-hoc test) after 4 days of continuous infection with a normal dose of spores is shown. **** = $p < 0.001$, ** = $p < 0.01$, * = $p < 0.05$, ns = not significant ($p > 0.05$)*. Data for each condition includes 3 biological replicates.

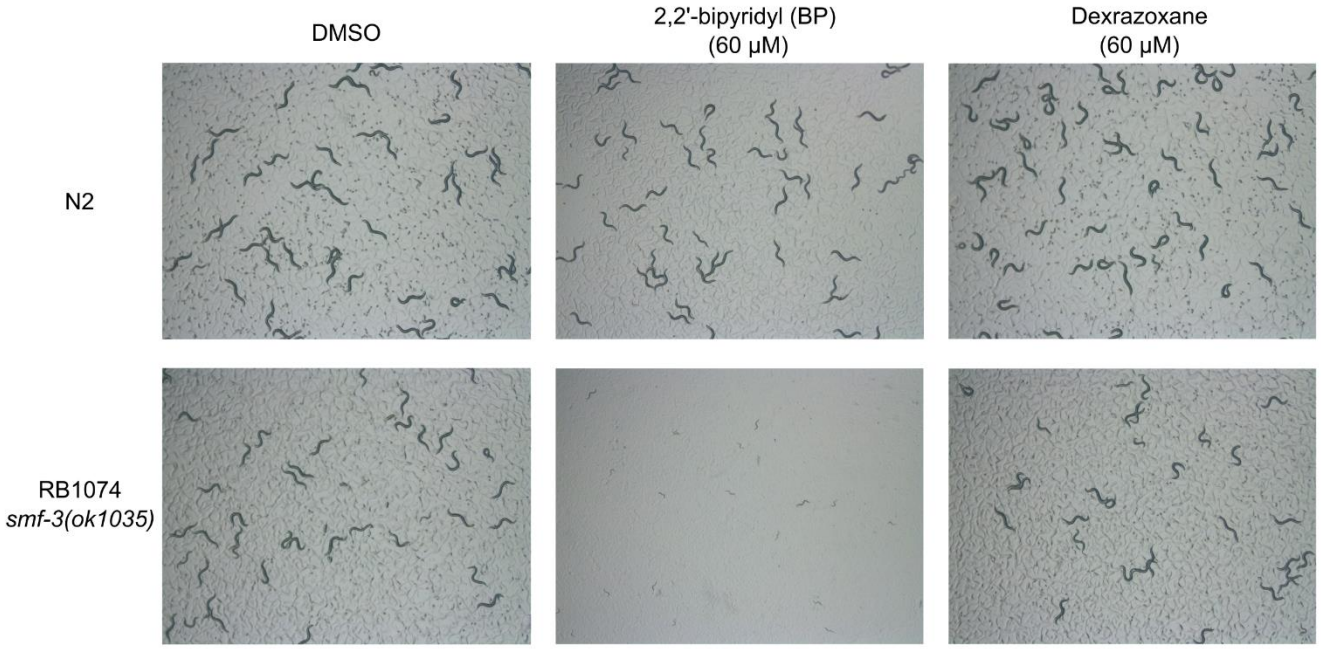

Figure S3. *C. elegans* mutant strain with reduced iron is not sensitive to dexrazoxane. RB1074 animals have 50% less iron compared to N2 and display severe growth defects during treatment with the iron chelator BP on NGM plates for 3 days from the L1 stage (bottom middle), but not after treatment with dexrazoxane (bottom right) (47).

Table S1: Initial screen hits, retest outcomes and available PubChem CIDs.

Compound	Retest Outcome	PubChem CID
Danthron	-	2950
Ethinyl Estradiol	+	5991
Methoxsalen	-	4114
Nebivolol Hydrochloride	-	9933004
Menadione	+	4055
Perhexiline Maleate	-	5284439
Clioquinol	-	2788
Securinine	-	442872
Parthenolide	+	108068
Methyl 7-desoxypurpurogallin-7-carboxylate trimethyl ether	-	4020695
Plumbagin	+	10205
Bisabolol	-	1549992
Chrysarobin	-	68111
Methyl Deoxycholate	-	229346
4-Nonylphenol	-	1752
Haematoporphyrin	-	11103
Curcumin	+	969516
Chloranil	+	8371
(-) E-Caryophyllene Hydrate	-	6429321
4,4'-Dimethoxydalbergione (Dalbergione)	+	364106
4,6-Dimethoxytoluquinone (Toluquinone)	+	NA
Thymoquinone	+	10281
Pyrogallin	-	822798
1-Benzyloxycarbonylaminophenethyl chloromethyl ketone (ZPCK)	+	99625
Dexrazoxane	+	71384